2022-05-12

Single extreme storm sequence can offset decades of shoreline retreat projected to result from sea-level rise

Harley, MD

http://hdl.handle.net/10026.1/19230

10.1038/s43247-022-00437-2
Communications Earth & Environment
Nature Research

SINGLE EXTREME STORM SEQUENCE CAN OFFSET DECADES OF SHORELINE RETREAT PROJECTED TO RESULT FROM SEA-LEVEL RISE

Mitchell D. Harley[1*], Gerd Masselink[2], Amaia Ruiz de Alegría-Arzaburu[3], Nieves G. Valiente[2,4], Tim Scott[2]

[1]Water Research Laboratory, School of Civil and Environmental Engineering, UNSW Sydney, Manly Vale, Australia
m.harley@unsw.edu.au
[2]Coastal Processes Research Group, School of Biological and Marine Sciences, University of Plymouth, Plymouth, United Kingdom
[3]Instituto de Investigaciones Oceanológicas, Universidad Autónoma de Baja California, Ensenada, Mexico
[4]Met Office, Exeter, United Kingdom

Abstract

Extreme storms cause extensive beach-dune erosion and are typically considered to enhance coastal erosion due to sea-level rise. However, extreme storms can also have a positive contribution to the nearshore sediment budget by exchanging sediment between the lower and upper shoreface and/or between adjacent headlands, potentially mitigating some adverse sea-level rise impacts. Here we use three high-resolution morphological datasets of extreme storm-recovery sequences from Australia, the UK and Mexico to quantify the nearshore sediment budget and relate these episodic volume changes to long-term coastal projections. We show that sediment gains over the upper shoreface were large (59–140 m^3/m) and sufficient to theoretically offset decades of projected shoreline retreat due to sea-level rise, even for a high-end greenhouse gas emissions scenario (SSP5-8.5). We conclude that increased confidence in shoreline projections relies fundamentally on a robust quantitative understanding of the sediment budget, including any major short-term sediment contribution by extreme storms.

Introduction

Climate change is likely to cause a global sea-level rise (SLR) by 2100 of 0.63–1.01 m based on a high-end greenhouse gas emissions scenario (SSP5-8.5)[1]. Combined with ambient trends in shoreline dynamics, SLR under this scenario has been projected (using an approach known as the Bruun rule[2]) to result in a large retreat or loss of almost half of the world's sandy beaches by the end of this century[3]. Climate change has also been predicted to drive increases in extreme wave heights along almost three fifths of the world's coastline by the end of the century[4], but the long-term (> 50 years) impact of extreme storms on coastal recession – and its coupling with SLR – is ambiguous. Increased storminess is generally assumed to exacerbate coastal erosion due to SLR; however, short-to-medium term (years–decades) shoreline variability caused by storms is generally considered noise over long time scales when shoreline change is mainly driven by SLR[5,6]. On the other hand, extreme storms can transport sediment into the nearshore zone from elsewhere, for example from the lower shoreface[7], potentially tempering long-term erosion by SLR[8,9].

Despite its many assumptions and shortcomings[10,11], the Bruun rule has emerged as the most widely used method for predicting shoreline change due to SLR[6], for localized coastal hazard assessments[12] as well as in global studies[3,13]. In its most simple and original form, the Bruun rule reduces to $R = S/\tan\beta$, where R is shoreline retreat, S is sea-level rise and $\tan\beta$ is the upper shoreface gradient. Application of the Bruun rule involves a simple upward and backward translation of the shoreface profile to a location where the volumetric losses from the upper part of the profile are matched by the gains across the lower part. Sediment gains and losses can be included in the Bruun rule[14,15], but their inclusion requires a rigorous insight into the nearshore sediment budget[16] as the cross-shore and longshore sediment fluxes, sediment production and anthropogenic contribution all play a key role in the coastal response. Of particular relevance in this context is the impact of extreme storm activity on the sediment budget, as it is under these forcing conditions that sediment fluxes are maximized and the impact of the sediment budget on long-term shoreline change is potentially greatest.

Coastal erosion and shoreline retreat as a result of extreme storm activity is particularly apparent on the upper beach as storm waves leave beaches depleted and coastal dunes scarped, with typical beach-dune sediment losses of 50–150 m^3 per unit meter beach width[17–19]. A suite of cross-shore and longshore sediment transport pathways are responsible for these morphological changes, summarized in Figure 1. The vast majority of sediment transport pathways during both extreme and non-energetic (i.e., modal) wave conditions merely redistribute sediment across the upper shoreface, i.e., landward of the depth of closure (DoC), defined as the depth beyond which no detectable morphological change occurs over a given timeframe[20–22]. Sediment exchange between the lower and upper shoreface across the DoC can, however, play an important role in long-term shoreline change, and of particular interest here is the wave-driven onshore sediment transport driven by disequilibrium shoreface morphology[7,9].

Geological evidence from Australia strongly suggests that low-magnitude onshore sediment transport $O(1\ m^3/m/yr)$ from the lower shoreface to the beach has been responsible for extensive coastal progradation when sea level was relatively stable throughout the mid to late Holocene[23–25] (see also examples from Brazil[26] and The Netherlands[27]). Under the influence of rising sea level, this component, which results in a lowering of the lower shoreface as sediment is transported onshore[28], has the potential to offset, or even overturn, the impact of sea-level rise[14]. As the source of this sediment is beyond the DoC, it is highly likely that energetic wave conditions are implicated in this transport, as modal waves are not expected to be able to move sediments at such depths. Onshore-skewed oscillatory motions on the seabed caused by wave nonlinearity are able to act at much greater depths during energetic conditions, providing a mechanism for suspended and bedload sediment transport from the lower to upper shoreface[29]. Net shoreface sand supply to beaches may be a widespread and common, but little appreciated factor in coastal stability[30,31]. Likewise, sediment from adjacent beaches and mobilised during extreme storms (e.g., headland sand bypassing) may provide an additional source of sediment to the nearshore region[32–34].

This paper presents three unique coastal morphological data sets from three different continents (Australia, Europe and North America, refer Figure 2) that each encompass a sequence of an extreme storm or extended storm cluster followed by a milder period of beach recovery. Despite the morphological data being collected beyond the theoretical DoC, sediment budget analysis unequivocally points towards unbalanced sediment budgets at all three sites, demonstrating in these cases large sediment gains within the upper shoreface over the storm-recovery sequence. We show that these short time-scale events can have important implications for long-term coastal evolution and, when placed in the context of projections undertaken using the common Bruun rule approach, can theoretically offset decades of predicted shoreline retreat due to SLR, even under a high-range greenhouse gas emissions scenario (SSP5-8.5). Our results highlight major limitations of the Bruun rule approach for long-term coastal projections and emphasize the need for enhanced shoreface monitoring worldwide to better quantify changes in sediment budgets due to climate change.

Results

Figures 3-5 summarize long-term and extreme storm sequence results at three high-resolution coastal monitoring locations in Australia, the UK and Mexico. These three locations are: (1) the 3.6 km-long Narrabeen embayment in SE Australia (Figure 3), comprising one of the longest (> 40 years, monthly) subaerial beach survey programs worldwide[35]; (2) the 3.5 km-long Perranporth embayment in SW England (Figure 4), where monthly subaerial beach surveys have been undertaken monthly since 2006[36]; and (3) the open-coast La Misión Beach in NW Mexico (Figure 5), where a 2.2-km stretch of sandy coast has been monitored monthly since 2015. Each site is characterized as wave-dominated (average $H_s \approx 1.6$ m at all three sites), sandy ($D_{50} \approx 0.3$–0.4 mm) and of moderate upper shoreface steepness ($\tan\beta$, ≈ 0.03–0.04). The tidal regimes at Narrabeen and La Misión are microtidal (spring tidal range = 1.3 and 2.3 m, respectively), whereas Perranporth is macrotidal (spring tidal range = 6.3 m).

Complementing the continuous subaerial beach measurement records (including dune systems if present) were detailed three-dimensional surveys of the entire upper shoreface at time intervals prior to, immediately following and approximately 12 months after an extreme storm event or extended storm cluster. At Narrabeen, an extreme east coast low storm impacted the coast in June 2016 that resulted in the largest subaerial beach erosion (average = 121 m^3/m) over four decades[19]. At Perranporth, a cluster of extratropical cyclones over successive boreal winters between 2013 and 2016 caused an average of 212 m^3/m of subaerial beach erosion, with the 2013/2014 winter period in particular considered the most energetic winter period since at least 1948[18]. At La Misión, a similar sequence of extratropical storms concentrated over the 2018/2019 boreal winter caused the most severe winter erosion (average = 208 m^3/m) since measurements at the site began (Figure 5b). Each three-dimensional survey extended from the upper beach to beyond the theoretical DoC over the respective storm sequences, calculated (see Methods) as -11.6 m (Narrabeen), -19.3 m (Perranporth) and -9.1 m (La Misión), all referenced to mean sea level (MSL).

The morphological response from all three storm sequences indicates patterns of extensive erosion along the subaerial beach coupled with adjacent sediment deposition in the shallow subaqueous zone. Representative cross-shore transects (Figures 3g, 4e and 5e) show these deposition zones are characterized by pronounced storm bar morphology with bar crests between approximately 200 m offshore for the microtidal Narrabeen site and 700 m for the macrotidal Perranporth site. Pivot points separating areas of upper-shoreface storm erosion and deposition are observed at depths relative to MSL of approximately -2.9 m (Narrabeen), -5.8 m (Perranporth) and -1.2 m (La

Misión). In the subsequent recovery phase, eroded sediment stored in the storm bar returns under more modal wave conditions, and the patterns of storm erosion and deposition are mostly reversed. At lower depths, profile variability displays the characteristic 'pinching' towards the theoretical DoC that is typical of the upper shoreface, although seabed variability outside of the survey error (~0.14 m) is still evident at these lower depths.

Integrating these observations over the upper shoreface and beach, whilst carefully considering survey error (refer Methods), reveals that the overall sediment balances are not closed and all three locations record large net sediment gains over the storm-recovery sequence (Figure 6). Average net gains per unit meter beach width range from +59 m^3/m (La Misión) to +140 m^3/m (Perranporth), which are comparable in magnitude to the extreme erosion observed over the subaerial beach during each storm sequence. In absolute terms, within the three-dimensional survey areas spanning several kilometres, these sediment gains equate to +130 000 m^3 of sediment (La Misión), +400 000 m^3 (Narrabeen) and +420 000 m^3 (Perranporth). While the direct source of these sediment gains cannot be conclusively ascertained without detailed process-based measurements and tracer experiments, the alongshore variability and phasing of these net gains provide some insight into the sediment pathways (using Figure 1 for reference). At Narrabeen, sediment gains occurred primarily in the storm phase and are strongly skewed towards the southern half of the embayment (max. net gain = +392 m^3/m). This is consistent with likely counter-clockwise beach rotation (Transport Pathway 3 in Figure 1) caused by this anomalous easterly storm[19,37], but also coincides with the region of the rocky embayment where lower shoreface sand bodies (i.e., beyond the DoC) are more abundant[38], suggesting onshore sediment transport from the lower to upper shoreface (Pathway 6). At Perranporth, sediment gains occurred instead primarily over the recovery phase and particularly at the southern half (max. net gain = +271 m^3/m), which might be related to alongshore headland sand bypassing input at the southern extremity (Pathway 1) under less-extreme winter periods that have been shown to enhance beach recovery[32]. Similar to Narrabeen, sediment gains at La Misión occur primarily over the storm phase, but unlike the embayed Narrabeen and Perranporth sites, shows no obvious alongshore bias (max. gain = +309 m^3/m). Possible sediment sources for these net gains include onshore sediment transport from lower shoreface sand storages (Pathway 6), as well as winter fluvial discharges from the nearby tidal inlet (Pathway 7).

The observed sediment gains over the entire upper shoreface and beach are subsequently characterized in terms of equivalent years of theoretical shoreline retreat predicted by the Bruun rule under various emission scenarios[1], thereby evaluating the potential for substantial errors in shoreline predictions due to SLR using the Bruun rule approach[14]. Figure 6b shows that the annual rate of sediment input required to theoretically offset 21st Century (2000–2100) SLR recession as predicted by the Bruun rule (Q_{offset}) is a function of the upper shoreface width W^*, defined as the horizontal distance from the subaerial beach berm to the DoC. Here we use the long-term DoC derived from 41 years of wave reanalysis data (see Methods), rather than over the DoC calculated over the shorter-term storm-sequence as above[28]. For Narrabeen, the narrower upper shoreface width (long term DoC = -14.3 m, W^* = 480 m) means that this offset rate equates to 3.7 m^3/m/year for SLR estimated under an upper SSP5-8.5 emissions scenario between 2000 and 2100, compared to 6.2 and 8.4 m^3/m/year for the deeper and wider La Misión and Perranporth upper shorefaces (long term DoC = -18.2 m and -20.2 m, W^* = 810 m and 1090 m for La Misión and Perranporth, respectively). Based on these annual rates, the observed sediment gains over the extreme storm-recovery sequence at Narrabeen are equivalent to 25 years of SLR recession predicted by the Bruun rule that may be theoretically offset at the upper SSP5-8.5 scenario, or 43 years for the more sustainable SSP1-2.6 emissions scenario. At Perranporth and La Misión, these sediment gains equate to 18 and 10 years for SSP5-8.5, or 31 and 17 years for SSP1-2.6, respectively.

Discussion

Our results based on unique high-resolution field measurements over three extreme storm-recovery sequences from three different continents highlight the present major challenges of predicting long-term coastal evolution over planning horizons of decades to centuries. Whereas long-term modelling approaches typically assume short-term sediment losses on the subaerial beach and dune caused by extreme storm sequences are balanced by sediment gains in the subaqueous zone (resulting in zero net change in the sediment budget), our results indicate large net positive sediment gains integrated over the entire upper shoreface. Furthermore, the magnitude of these observed net gains – which primarily manifest at depths from MSL down to the DoC – are commensurate ($O(100\ m^3/m)$) to the extreme erosion that is highly visible (and widely-reported[18,19]) on the subaerial beach and dune during these extreme events. Likewise, these magnitudes equate to typical volumes undertaken for artificial beach nourishment projects[39] and, when expressed in terms of Bruun-rule predicted shoreline change, are equivalent to offsetting decades of predicted shoreline retreat, even under an upper-range emissions scenario (SSP5-8.5). This highlights the potential for a cascading of model prediction error using the Bruun rule and other simplified approaches (e.g., [9,23]) that do not implicitly include storm-driven sediment fluxes, placing additional concern[10,11] regarding their validity for long-term prediction. This is particularly in light of robust projections pointing towards an increase in extreme waves along almost three fifths of the world coastline[4], implying an exacerbation of episodic major sediment exchange between the lower and upper shoreface, and/or alongshore adjacent embayments, in the coming decades that could significantly alter long-term coastal evolution.

Whether these observed major short-term net sediment gains to the upper shoreface and beach are relatively common, or indicative of the extreme nature of these particular storm sequences, is presently difficult to ascertain. Each storm sequence is characterized by extreme subaerial beach erosion that equates to the largest short-term erosion volumes observed in this upper part of the beach over their respective measurement records (refer Figures 3c, 4b and 5b). At lower depths, however, the potential for major wave-driven sediment transport across the DoC (i.e., Pathway 6 in Figure 1) can be evaluated by estimating wave orbital velocities (U_{rms}) at the seabed corresponding to the long-term DoC (see Methods). This simple approach provides a first-order assessment of sediment transport potential, while recognising that processes such as longshore sediment transport and headland bypassing (Pathway 1), upwelling and/or tidal currents (Pathway 9) and estuarine/fluvial inputs (Pathway 7) may all play a key role[22,29]. Figure 7 indicates that for the three respective storm sequences, wave orbital velocities at these depths are estimated to have reached up to 1.2 m/s (Perranporth), 1.0 m/s (Narrabeen) and 0.6 m/s (La Misión), which are well above the typical threshold of motion for shoreface sediment ($U_{\mathrm{crit}} \approx 0.2$ m/s, see Methods) and suggest large sediment transport potential. Over the longer-term (1979–2020) dataset, these equivalent wave orbital velocities are estimated to occur only rarely at Perranporth and Narrabeen where the largest net sediment gains were observed (ΔV = +140 m^3/m and +91 m^3/m, respectively), having been exceeded just 9 hours over the 41-year record at Perranporth (i.e., U_{rms} > 1.2 m/s) and 91 hours at Narrabeen (U_{rms} > 1.0 m/s). At La Misión, where observed net sediment gains were the smaller of the three sites (ΔV = +59 m^3/m), equivalent wave orbital velocities are estimated to occur more frequently over the historical record (636 hours over the 41 years, U_{rms} > 0.6 m/s). This suggests a potential scaling between sediment transport potential (estimated by the wave orbital velocity at the DoC) and the magnitude of short-term net sediment gains caused by storm-recovery sequences, with less-frequent events potentially resulting in a larger sediment influx. A notable example evident in the historical dataset at La Misión is the January 1988 storm (maximum U_{rms} = 1.4 m/s, Figure 7c) that resulted in extreme coastal impacts at nearby Southern California, including reported *in situ* observations[40] of large seabed changes extending down to depths of -25 m.

Further evidence as to the historical frequency of these major short-term net sediment gains can be garnered from the long-term subaerial volume measurements. Considering the Narrabeen beach monitoring program that spans 44 years of continuous subaerial beach measurements[35], the subaerial beach volume data (Figure 3c) indicate no significant long-term erosion or accretion trend (linear regression trend = -0.08 ± 0.11 m^3/m/year). Similar to the wave orbital velocity analysis above, this suggests that similar short-term sediment gains as observed over the 2016-2017 storm-recovery sequence at this site have either: (1) occurred very rarely; (2) do not have a noticeable subaerial beach signature (i.e., sediment gains do not move sufficiently onshore to be observed on the subaerial beach); have been balanced by equivalent sediment losses (e.g., Pathways 1, 7, 8 and 9 in Figure 1); or (3) have possibly contributed to offsetting the approximately 0.10 m of relative SLR that has occurred over this 44-year record[41]. At Perranporth and La Misión, the subaerial beach volume data suggest a slight erosional trend at Perranporth (linear regression trend = -5.3 ± 2.9 m^3/m/year) and a relatively strong accretionary trend at La Misión (linear regression trend = 23.3 ± 16.8 m^3/m/year), although it is likely that these shorter-term records are biased by the storm sequences themselves.

While each of the three datasets show net positive sediment contributions, equally plausible on sandy coastlines more generally are extreme storm sequences that cause major losses to the overall sediment budget (e.g. imbalances in Pathways 1, 7, 8 and 9 in Figure 1). Short-term sediment fluxes between the lower and upper shoreface (across the DoC) and from adjacent beaches reflect complex interactions between sediment transport processes, sediment storage (both on the lower shoreface and at adjacent beaches) and accommodation space between the lower and upper shoreface. As outlined in two recent reviews of shoreface morphodynamics[29,42], the present conceptual understanding of sediment transport on the lower shoreface is extremely limited. This is due to a combination of many factors, including: subtle imbalances between onshore and offshore-directed sediment fluxes; the dominance of bed load and gravity flows at these depths; the presence of migrating bedforms; a paucity of field data measurements beyond the surf zone; and uncertainties associated with up-scaling short-term measurements and process understanding to longer time scales. These limitations are compounded by the severe lack of any knowledge of the seabed composition on the lower shoreface, with estimates suggesting that 71% of ocean depths between the MSL and -200 m depth contours remain completely uncharted[43].

Predicting the potential fate of coastal environments out to the year 2100 and beyond, i.e., forecasting the 2100 coastline, is one of the most pressing challenges facing coastal science today. While it is unlikely that a step-change in our ability to model sediment transport at and between the lower and upper shoreface will be achieved in the near future, significant improvements in long-term predictions can be realised through: (1) a major upscaling of seabed mapping efforts (e.g. [44,45]) to evaluate the magnitude of sediment presently stored on the lower shoreface; and (2) a significantly greater number of routine monitoring efforts of entire nearshore systems appropriate for quantifying sediment fluxes. These two steps can greatly help identify both short and long-term changes to sediment budgets and their connectivity between lower and upper shoreface (including dunes), and between adjacent embayments, as well as provide early warning for coastal communities of any large-scale sediment shifts to SLR in the coming decades. The latter is particularly important considering potential coastal barrier overstepping and dramatic shoreline change under very rapid sea-level rise scenarios, as has been observed in the mid-Holocene[46]. Improvements in remote sensing technology (e.g. satellite-derived bathymetry[47]) are also likely to complement shoreface monitoring efforts, by providing regional perspectives on entire sediment compartments and their linkages[48]. However, the vertical accuracies of these technologies are still limited (σ_v > 0.4 m), re-emphasising the need for enhanced traditional *in-situ* monitoring strategies[49].

Methods

Multimethod morphological surveys

Morphological surveys at each of the three locations were undertaken using a combination of survey methods to ensure seamless digital elevation models (DEMs) spanning the subaerial and subaqueous beach system. At Narrabeen, subaerial beach surveys were undertaken using Airborne Lidar and Uncrewed Aerial Vehicles (UAVs), with vertical uncertainty (σ_v) quantified for this site and equipment as 0.11 m and 0.07 m, respectively[50,51]. At Perranporth, subaerial beach surveys were undertaken using a combination of Airborne Lidar (σ_v = 0.15 m) and either UAV (σ_v = 0.06 m at this site) or RTK-GNSS mounted to an ATV (σ_v = 0.05 m)[32]. At La Misión, subaerial beach surveys were undertaken by walking RTK-GNSS (σ_v = 0.05 m) at 50-m spaced cross-shore transects. At all three sites, subaqueous surveys were undertaken using a single beam echosounder mounted on a boat (Perranporth, σ_v = 0.05 m) or jetski (Narrabeen and La Misión, σ_v = 0.10 m). These depth soundings were collected near-continuously along cross-shore transects spaced every 50 m at Narrabeen and Perranporth, or every 150 m at La Misión. At Perranporth, surveys were also complemented in deeper water (< -10 m) by multibeam echosounder (σ_v = 0.06–0.30 m)[32]. Seamless DEMs were subsequently created from the multimethod surveys using cubic interpolation. This method was found to best represent natural beach variability (e.g. intertidal bars) in the small data gaps (<30 m cross-shore) between subaerial and subaqueous measurements found at the microtidal Narrabeen and La Misión sites.

Sediment budget error analysis

DEMs of Difference (DoD), characterizing spatial variability in beach elevation change at each site, were calculated from the individual DEMs described above. Sediment budget error analyses were calculated following the approach of [52], by first considering the limit of detection (*LoD*) for each DEM grid point:

$$LoD = \sqrt{\sigma_{\mathrm{DEM1}}{}^{2} + \sigma_{\mathrm{DEM2}}{}^{2}}$$

where σ_{DEM} is the vertical uncertainty at each grid point depending on the localized survey method. The overall volume change ΔV and associated uncertainty for each DoD were then calculated by considering only statistically-significant (95% confidence level) morphological change above the limit of detection ($|Z_{\mathrm{DEM1}} - Z_{\mathrm{DEM2}}| > LoD$). These overall volume changes ΔV were then normalized per unit beach width based on the number of cross-shore transects in the survey region.

Equivalent years of SLR recession theoretically offset using the Bruun rule

Volumetric changes to the sediment budget caused by the three storm sequences were converted to equivalent years of SLR recession that may be theoretically offset over the 21st Century when estimated using the Bruun rule, in order to evaluate the potential for large error using this simple approach. Upper shoreface widths W^* were calculated at each site considering the alongshore-averaged horizontal distance between the subaerial beach berm and the long-term *DoC*, which is calculated relative to mean low water as[21,53]:

$$DoC = 2.28H_{\mathrm{s},Y} - 68.5\left(\frac{H_{\mathrm{s},Y}{}^{2}}{gT_{\mathrm{p},Y}{}^{2}}\right)$$

where $H_{s,Y}$ is the significant wave height exceeded 12 hours every Y years, g is gravity and $T_{p,Y}$ the associated peak wave period. Following other SLR estimates using the Bruun rule (e.g., [3,13]), ERA5 wave reanalysis data[54] spanning 41 years (1979–2020) was used to calculate the long-term DoC at each site. These values relative to mean low water were then converted to MSL considering the tidal range. The annual rate of sediment input required to theoretically offset SLR recession using the Bruun rule (Q_{offset}) is subsequently calculated by:

$$Q_{offset} = \frac{S}{Y}W^{*}$$

where S is the predicted median change in sea level over the 21st Century[1] (S = 0.44 m and 0.77 m for SSP1-2.6 and SSP5-8.5 scenarios for 2000–2100, respectively) and Y the time period in years (Y = 100 years). The equivalent years of SLR recession that may be theoretically offset is then calculated by dividing the volumetric changes ΔV by Q_{offset}.

Orbital wave velocities at the depth of closure

Orbital wave velocities (U_{rms}) at the DoC for each of the three sites were estimated to assess sediment transport potential at these depths from the historical ERA5 wave reanalysis between 1970 and 2020. The wave orbital velocity can be estimated from random waves (assuming a JONSWAP spectrum) by an explicit solution defined by[55]:

$$U_{\mathrm{rms}} = \frac{0.25H_{\mathrm{s}}}{T_n(1 + At^2)^3}$$

$$A = [6500 + (0.56 + 15.54t)^6]^{\frac{1}{6}}$$

$$T_n = \left(\frac{Z_{\mathrm{DoC}}}{g}\right)^{\frac{1}{2}}$$

$$t = \frac{T_n}{T_{\mathrm{z}}}$$

where Z_{DoC} is the seabed depth corresponding to the long-term DoC (Narrabeen = -14.3 m, Perranporth = -20.2 m, La Misión = -18.2 m), H_s the significant wave height (from ERA5 reanalysis) and T_z the zero-crossing wave period. T_z is calculated from the ERA5 peak wave period T_p using the spectral approximation $T_z \approx 0.78 T_p$. The typical threshold of motion for shoreface sediment resulting from wave orbitals at the seabed is estimated based on a characteristic wave period of 10s and shoreface sediment in the range D_{50} = 0.2-0.7 mm (refer Figure 19 in [56]).

Data Availability

The data that support the findings of this study are available for download at https://doi.org/10.5281/zenodo.5748645. Narrabeen-Collaroy survey program data is available at http://narrabeen.wrl.unsw.edu.au/.

Code Availability

The code to analyse and plot the survey data in this study (written in MATLAB) is available upon request from the corresponding author.

Acknowledgements

This study was supported by the Australian Research Council (Grant #DP150101339), the UK Natural Environment Research Council (Grant NE/M004996/1; BLUE-coast project), CONACyT (CB-2014-238765 and INFR-2013-011005) and the UC-MEXUS CN-18-179 project. Narrabeen survey data was collected with the support of UNSW Aviation (Airborne Lidar) and the NSW Department of Planning, Industry and Environment (bathymetric data). Perranporth survey data was collected thanks to the efforts of numerous generations of PhD students and researchers from the Coastal Processes Research Group, University of Plymouth. La Misión data was collected thanks to the support of the Coastal Morphodynamics Research Group, Universidad Autónoma de Baja California. The authors would like to acknowledge traditional owners on whose lands the research was undertaken.

Author Contributions

M.D.H and G.M. conceptualized the study and led the writing of the manuscript. M.D.H. led the survey data collection at Narrabeen and undertook the data analysis at Narrabeen and La Misión. G.M., N.V. and T.S. led the survey data collection and analyses at Perranporth. A.R.A-A led the survey data collection and analysis at La Misión. All authors contributed to the writing of the manuscript.

References

1. Fox-Kemper, B. *et al.* Ocean, Cryosphere and Sea Level Change. in *Climate Change 2021: The Physical Science Basis. Contribution of Working Group I to the Sixth Assessment Report of the Intergovernmental Panel on Climate Change* (eds. Masson-Delmotte, V. et al.) (Cambridge University Press, 2021).

2. Bruun, P. Sea-Level Rise as a Cause of Shore Erosion. *Journal of the Waterways and Harbors Division* **88**, (1962).

3. Vousdoukas, M. I. *et al.* Sandy coastlines under threat of erosion. *Nature Climate Change* **10**, 260–263 (2020).

4. Meucci, A., Young, I. R., Hemer, M., Kirezci, E. & Ranasinghe, R. Projected 21st century changes in extreme wind-wave events. *Science Advances* **6**, 1–10 (2020).

5. Vitousek, S., Barnard, P. L., Limber, P., Erikson, L. & Cole, B. A model integrating longshore and cross-shore processes for predicting long-term shoreline response to climate change. *Journal of Geophysical Research: Earth Surface* **122**, 782–806 (2017).

6. D'Anna, M., Idier, D., Castelle, B., Vitousek, S. & le Cozannet, G. Reinterpreting the Bruun rule in the context of equilibrium shoreline models. *Journal of Marine Science and Engineering* **9**, (2021).

7. Kinsela, M. A., Daley, M. J. A. & Cowell, P. J. Origins of Holocene coastal strandplains in Southeast Australia: Shoreface sand supply driven by disequilibrium morphology. *Marine Geology* **374**, 14–30 (2016).

8. Cowell, P. J., Thom, B. G., Jones, R. A., Everts, C. H. & Simanovic, D. Management of uncertainty in predicting climate-change impacts on beaches. *Journal of Coastal Research* **22**, 232–245 (2006).

9. Aagaard, T. & Hughes, M. G. Equilibrium shoreface profiles: A sediment transport approach. *Marine Geology* **390**, 321–330 (2017).

10. Cooper, J. A. G. & Pilkey, O. H. Sea-level rise and shoreline retreat: Time to abandon the Bruun Rule. *Global and Planetary Change* **43**, 157–171 (2004).

11. Cooper, J. A. G. *et al.* Sandy beaches can survive sea-level rise. *Nature Climate Change* **10**, 993–995 (2020).

12. Wainwright, D. J. *et al.* Moving from deterministic towards probabilistic coastal hazard and risk assessment: Development of a modelling framework and application to Narrabeen Beach, New South Wales, Australia. *Coastal Engineering* **96**, 92–99 (2015).

13. Athanasiou, P. *et al.* Global distribution of nearshore slopes with implications for coastal retreat. *Earth System Science Data Discussions* 1–29 (2019).

14. Dean, R. G. & Houston, J. R. Determining shoreline response to sea level rise. *Coastal Engineering* **114**, 1–8 (2016).

15. McCarroll, R. J. *et al.* A rules-based shoreface translation and sediment budgeting tool for estimating coastal change: ShoreTrans. *Marine Geology* **435**, 106466 (2021).

16. Rosati, J. D. Concepts in sediment budgets. *Journal of Coastal Research* **21**, 307–322 (2005).

17. Castelle, B., Bujan, S., Ferreira, S. & Dodet, G. Foredune morphological changes and beach recovery from the extreme 2013/2014 winter at a high-energy sandy coast. *Marine Geology* **385**, 41–55 (2017).

18. Masselink, G. *et al.* Extreme wave activity during 2013/2014 winter and morphological impacts along the Atlantic coast of Europe. *Geophysical Research Letters* **43**, 2135–2143 (2016).

19. Harley, M. D. *et al.* Extreme coastal erosion enhanced by anomalous extratropical storm wave direction. *Scientific Reports* 1–9 (2017).

20. Udo, K., Ranasinghe, R. & Takeda, Y. An assessment of measured and computed depth of closure around Japan. *Scientific Reports* **10**, 1–8 (2020).

21. Hallermeier, R. J. A profile zonation for seasonal sand beaches from wave climate. *Coastal Engineering* **4**, 253–277 (1981).

22. Valiente, N. G., Masselink, G., Scott, T., Conley, D. & McCarroll, R. J. Role of waves and tides on depth of closure and potential for headland bypassing. *Marine Geology* **407**, 60–75 (2019).

23. Cowell, P. J., Roy, P. S. & Jones, R. A. Simulation of large-scale coastal change using a morphological behaviour model. *Marine Geology* **126**, 45–61 (1995).

24. Thom, B. G. Transgressive and regressive stratigraphies of coastal sand barriers in southeast Australia. *Marine Geology* **56**, 137–158 (1984).

25. Oliver, T. S. N. *et al.* Holocene evolution of the wave-dominated embayed Moruya coastline, southeastern Australia: Sediment sources, transport rates and alongshore interconnectivity. *Quaternary Science Reviews* **247**, 106566 (2020).

26. Dillenburg, S. & Hesp, P. A. *Geology and Geomorphology of Holocene Coastal Barriers of Brazil*. (Springer-Verlag Berlin Heidelberg, 2009).

27. Beets, D. J. & van der Spek, A. J. F. The Holocene evolution of the barrier and the back-barrier basins of Belgium and the Netherlands as a function of late Weichselian morphology, relative sea-level rise and sediment supply. *Geologie en Mijnbouw/Netherlands Journal of Geosciences* **79**, 3–16 (2000).

28. Stive, M. J. F. & de Vriend, H. J. Modelling shoreface profile evolution. *Marine Geology* **126**, 235–248 (1995).

29. Anthony, E. J. & Aagaard, T. The lower shoreface: Morphodynamics and sediment connectivity with the upper shoreface and beach. *Earth-Science Reviews* **210**, 103334 (2020).

30. Cowell, P. J. *et al.* Shoreface Sand Supply to Beaches. in *Proceedings 27th International Conference on Coastal Engineering* 2495–2508 (2000).

31. Stive, M. J. F., Roelvink, D. J. A. & de Vriend, H. J. Large-scale coastal evolution concept. The Dutch coast. Paper No. 9. *Proceedings of the Coastal Engineering Conference* **2**, 1962–1974 (1991).

32. Valiente, N. G., McCarroll, R. J., Masselink, G., Scott, T. & Wiggins, M. Multi-annual embayment sediment dynamics involving headland bypassing and sediment exchange across the depth of closure. *Geomorphology* **343**, 48–64 (2019).

33. Silva, A. P. da *et al.* Headland bypassing timescales: Processes and driving forces. *Science of the Total Environment* **793**, 148591 (2021).

34. Fruergaard, M., Andersen, T. J., Johannessen, P. N., Nielsen, L. H. & Pejrup, M. Major coastal impact induced by a 1000-year storm event. *Scientific Reports* **3**, 1–7 (2013).

35. Turner, I. L. *et al.* A multi-decade dataset of monthly beach profile surveys and inshore wave forcing at Narrabeen, Australia. *Scientific Data* **3**, (2016).

36. Valiente, N. G. *et al.* Nearshore sediment pathways and potential sediment budgets in embayed settings over a multi-annual timescale. *Marine Geology* **427**, 106270 (2020).

37. Mortlock, T. R., Goodwin, I. D., McAneney, J. K. & Roche, K. The June 2016 Australian East Coast Low: Importance of wave direction for coastal erosion assessment. *Water* **9**, 1–22 (2017).

38. Albani, A. D., Rickwood, P. C., Quilty, P. G. & Tayton, J. W. The morphology and late Quaternary paleogeomorphology of the continental shelf off Sydney, NSW. *Australian Journal of Earth Sciences* **62**, 681–694 (2015).

39. de Schipper, M. A., Ludka, B. C., Raubenheimer, B., Luijendijk, A. P. & Schlacher, T. A. Beach nourishment has complex implications for the future of sandy shores. *Nature Reviews Earth and Environment* **2**, 70–84 (2021).

40. Dayton, P. K., Tegner, M. J., Seymour, R. J. & Parnell, P. E. Unusual County Marine Erosion in San Diego from a Single Storm. *Estuarine, Coastal and Shelf ScienceScience* **29**, 151–160 (1989).

41. Watson, P. J. Updated Mean Sea-Level Analysis: Australia. *Journal of Coastal Research* **36**, 915–931 (2020).

42. Hamon-Kerivel, K., Cooper, A., Jackson, D., Sedrati, M. & Guisado Pintado, E. Shoreface mesoscale morphodynamics: A review. *Earth-Science Reviews* **209**, (2020).

43. Mayer, L. *et al.* The Nippon Foundation-GEBCO seabed 2030 project: The quest to see the world's oceans completely mapped by 2030. *Geosciences* **8**, (2018).

44. Linklater, M. *et al.* Techniques for classifying seabed morphology and composition on a subtropical-temperate continental shelf. *Geosciences (Switzerland)* **9**, (2019).

45. Diesing, M. *et al.* Mapping seabed sediments: Comparison of manual, geostatistical, object-based image analysis and machine learning approaches. *Continental Shelf Research* **84**, 107–119 (2014).

46. Cooper, J. A. G. *et al.* Sandy barrier overstepping and preservation linked to rapid sea level rise and geological setting. *Marine Geology* **382**, 80–91 (2016).

47. Traganos, D., Poursanidis, D., Aggarwal, B., Chrysoulakis, N. & Reinartz, P. Estimating satellite-derived bathymetry (SDB) with the Google Earth Engine and sentinel-2. *Remote Sensing* **10**, 1–18 (2018).

48. Thom, B. G. *et al.* National sediment compartment framework for Australian coastal management. **154**, 103–120 (2018).

49. Turner, I. L., Harley, M. D., Almar, R. & Bergsma, E. W. J. Satellite optical imagery in Coastal Engineering. *Coastal Engineering* **167**, 103919 (2021).

50. Middleton, J. H. *et al.* Resolution and accuracy of an airborne scanning laser system for beach surveys. *Journal of Atmospheric and Oceanic Technology* **30**, 2452–2464 (2013).

51. Turner, I. L., Harley, M. D. & Drummond, C. D. UAVs for coastal surveying. *Coastal Engineering* **114**, 19–24 (2016).

52. Wheaton, J. M., Brasington, J., Darby, S. E. & Sear, D. A. Accounting for uncertainty in DEMs from repeat topographic surveys: Improved sediment budgets. *Earth Surface Processes and Landforms* **35**, 136–156 (2010).

53. Nicholls, R. J., Birkemeier, W. A. & Lee, G. Evaluation of depth of closure using data from Duck, NC, USA. *Marine Geology* **148**, 179–201 (1998).

54. Hersbach, H. *et al.* The ERA5 global reanalysis. *Quarterly Journal of the Royal Meteorological Society* **146**, 1999–2049 (2020).

55. Soulsby, R. L. & Smallman, J. V. *A direct method of calculating bottom orbital velocity under waves*. (HR Wallingford, 1986)

56. Soulsby, R. Threshold of Motion. In *Dynamics of Marine Sands* 97–110 (Thomas Telford Publishing, 1997).

Figure 1. Key sediment transport pathways under modal and extreme wave conditions on an embayed sandy beach. Red arrows denote sediment transport pathways during extreme storm conditions and black arrows during less-energetic modal conditions. Example cross-sections at three locations in the beach compartment are: **A.** a rocky headland with sandy bed above the depth of closure (DoC); **B.** a completely sandy beach system; and **C.** a rocky headland with sandy bed below the depth of closure.

Figure 2. Location and representative photos of the three study sites spanning three continents. a. Global map indicating location of the three study sites. Representative UAV images of the three sites are indicated for **b.** Narrabeen, Australia (photo: Mitchell Harley); **c.** Perranporth, UK (photo: Tim Scott); and **d.** La Mision, Mexico (photo: Amaia Ruiz de Alegría-Arzaburu).

Figure 3. **Summary of wave and entire beach variability at Narrabeen Beach, Australia. a.** Deep-water significant wave height for Sydney (1979–2020); and **b.** during the storm-recovery sequence. **c.** Average subaerial volume change from long-term surveys (1979–2020); and **d.** during the storm-recovery sequence. **e.** Overall vertical change due to the storm period and **f.** during the recovery period (Depth of Closure indicated by yellow solid lines). **g.** A representative cross-shore transect indicating pre-storm, post-storm and recovery morphology; and **h.** the vertical change over these two periods. Shaded regions in panels **a** and **c** denote the storm-recovery sequence and triangles in **b** and **d** the timing of pre-storm (blue), post-storm (red) and recovery (green) surveys. Basemap data in **e** and **f** ©2022 Nearmap.

Figure 4. **Summary of wave and entire beach variability at Perranporth, UK. a.** Deep-water significant wave height for Perranporth spanning the period of long-term beach surveys (2006–2020). **b.** Average subaerial volume change from beach surveys. Triangles in **a** and **b** represent the timing of pre-storm (blue), post-storm (red) and recovery (green) surveys. **c.** Overall vertical change during the storm period; and **d.** during the recovery period (Depth of Closure indicated by solid yellow line). **e.** A representative cross-shore transect indicating pre-storm, post-storm and recovery morphology; and **f.** the vertical change over these two periods. Note that the abrupt vertical change ($\Delta Z< -3$ m) indicated during the storm period is due to frontal dune erosion caused by the storm sequence Basemap data in **c** and **d** ©2022 Google (Imagery ©2022 CNES/Airbus).

Figure 5. **Summary of wave and entire beach variability at La Misión, Mexico. a.** Deep-water significant wave height for La Misión (2015–2020) spanning the period of beach surveys. **b.** Average subaerial volume change from beach surveys. Triangles in **a** and **b** denote the timing of pre-storm (blue), post-storm (red) and recovery (green) surveys. **c.** Overall vertical change during the storm period; and **d.** during the recovery period (Depth of Closure indicated by solid yellow line). **e.** A representative cross-shore transect indicating pre-storm, post-storm and recovery

morphology; and **f.** the vertical change over these two periods. Basemap data in **c** and **d** © 2022 Google (Imagery ©2022 Maxar Technologies).

Figure 6. Overall sediment budget changes due to extreme storm-recovery sequences can offset up to decades of predicted shoreline retreat due to sea-level rise. a. Alongshore averaged volume change (per unit metre) for Narrabeen (NAR), Perranporth (PPT) and La Misión (MIS) beaches are indicated for the storm and recovery periods, separated into subaerial (SUBAR), subaqueous (SUBAQ) and overall net change (NET). Error bars denote the 95% confidence interval for calculated volume changes considering survey error. **b.** The annual rate of sediment input required to theoretically offset predicted SLR recession over the 21st Century using the Bruun rule (Q_{offset}) for the three sites under SSP1-2.6 and SSP5-8.5 scenarios; and **c.** the equivalent years of 21st Century SLR that may be theoretically offset due to the net volumetric gains over each total period.

Figure 7. Estimates of historical sediment transport potential at the depth of closure. Wave orbital velocities (U_{rms}) at the depth of closure (DoC) are derived from ERA5 wave reanalysis (1979-2020) at each of the three study sites: **a.** Narrabeen, Australia; **b.** Perranporth, United Kingdom; and **c.** La Misión, Mexico. Shaded regions denote the storm-recovery sequences at the three sites, with darker regions corresponding to the storm periods and lighter regions the recovery periods. Coloured triangles indicate the timing of pre-storm (blue), post-storm (red) and recovery (green) surveys. As an indication of potential sediment transport, the approximate critical threshold of motion for typical shoreface sediment ($U \approx 0.2$ m/s) is indicated as a red dashed line.

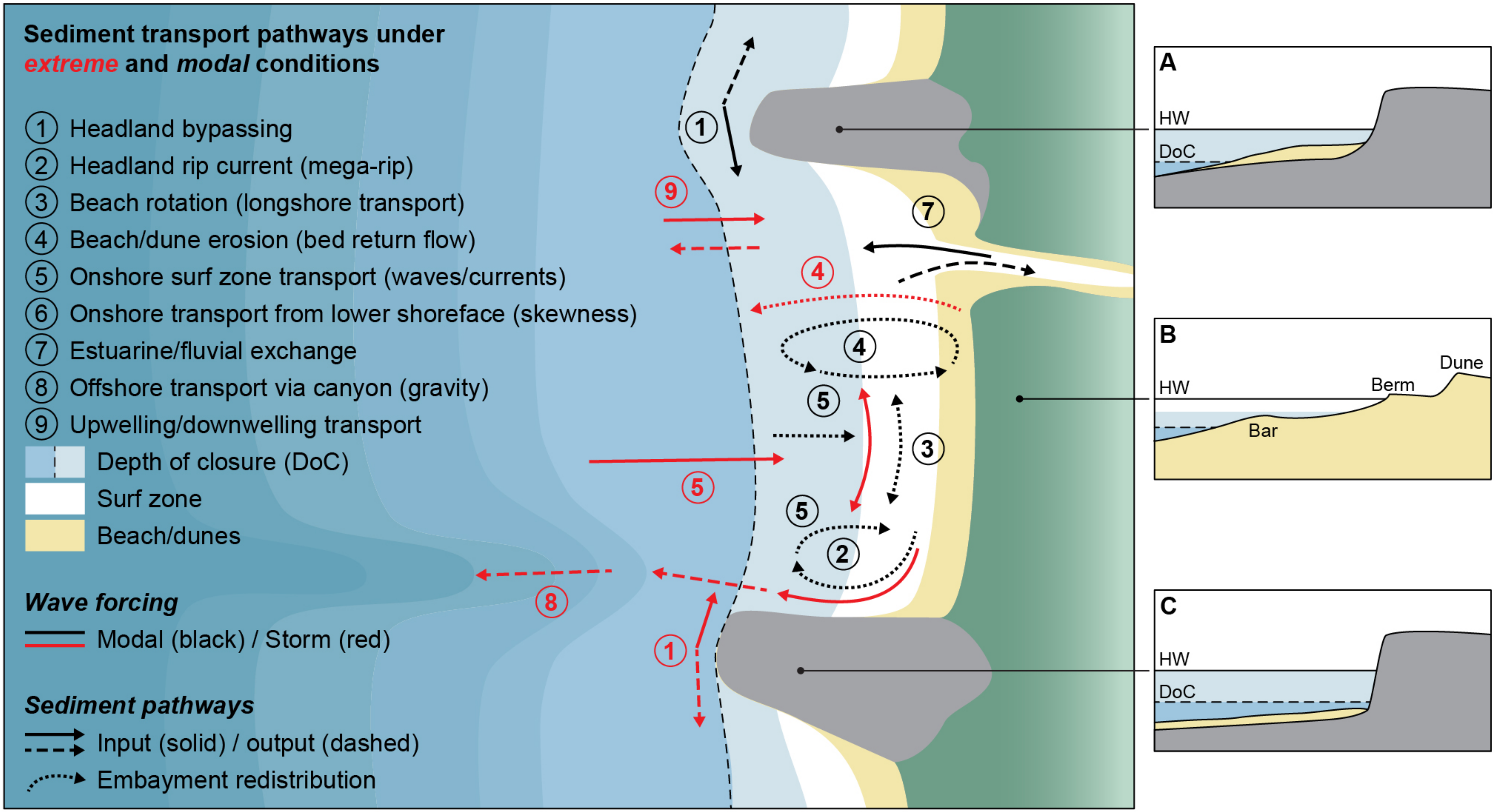

Sediment transport pathways under
extreme and modal conditions
1 Headland bypassing
2 Headland rip current (mega-rip)
3 Beach rotation (longshore transport)
4 Beach/dune erosion (bed return flow)
5 Onshore surf zone transport (waves/currents)
6 Onshore transport from lower shoreface (skewness)
7 Estuarine/fluvial exchange
8 Offshore transport via canyon (gravity)
9 Upwelling/downwelling transport
Depth of closure (DoC)
Surf zone
Beach/dunes
Wave forcing
Modal (black) / Storm (red)
Sediment pathways
Input (solid) / output (dashed)
Embayment redistribution
1
9
7
4
4
5
3
5
5
2
8
1
A
HW
DoC
B
HW
Berm
Dune
Bar
C
HW
DoC

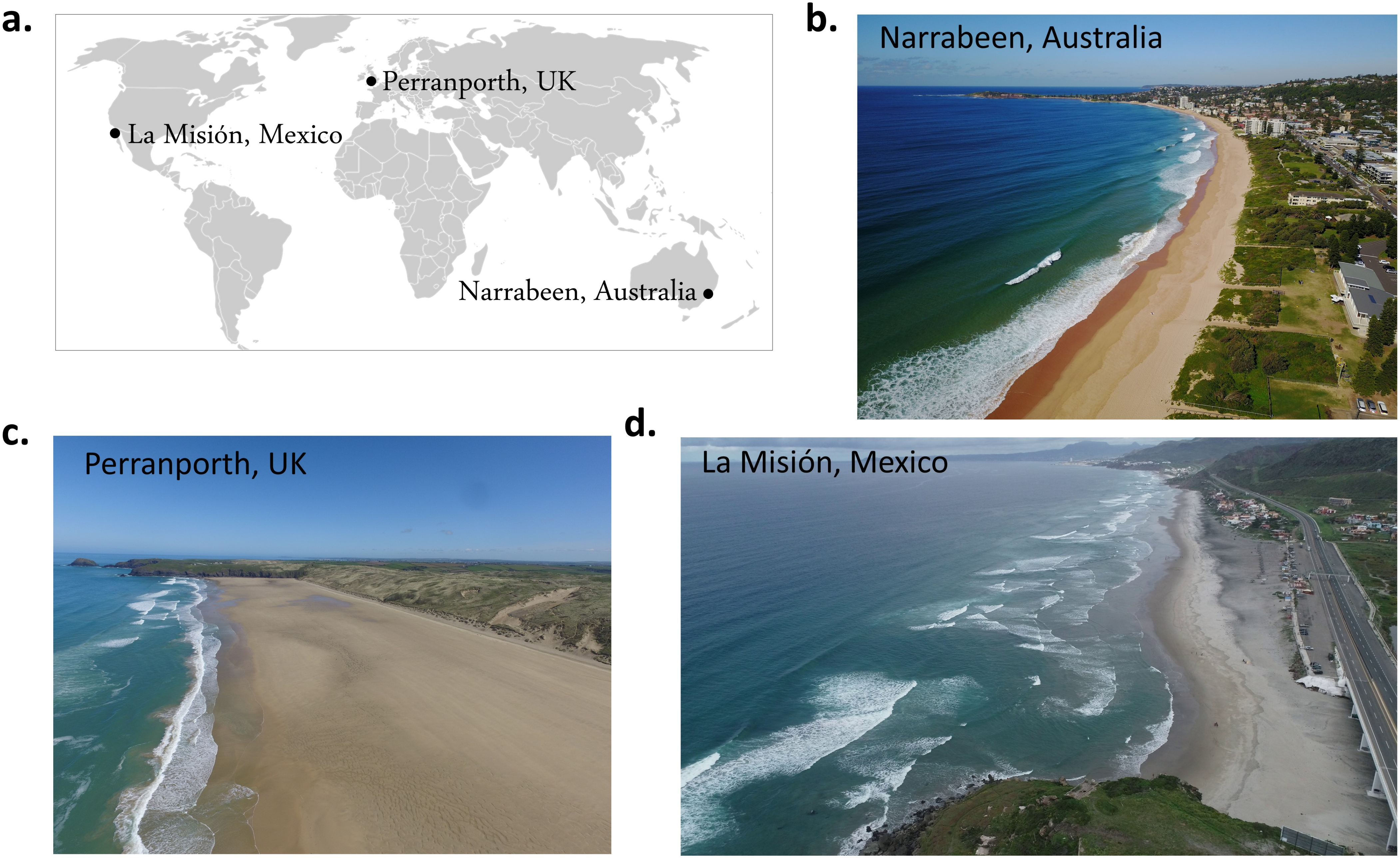
a.
Perranporth, UK
La Misión, Mexico
Narrabeen, Australia
b.
Narrabeen, Australia
c.
Perranporth, UK
d.
La Misión, Mexico

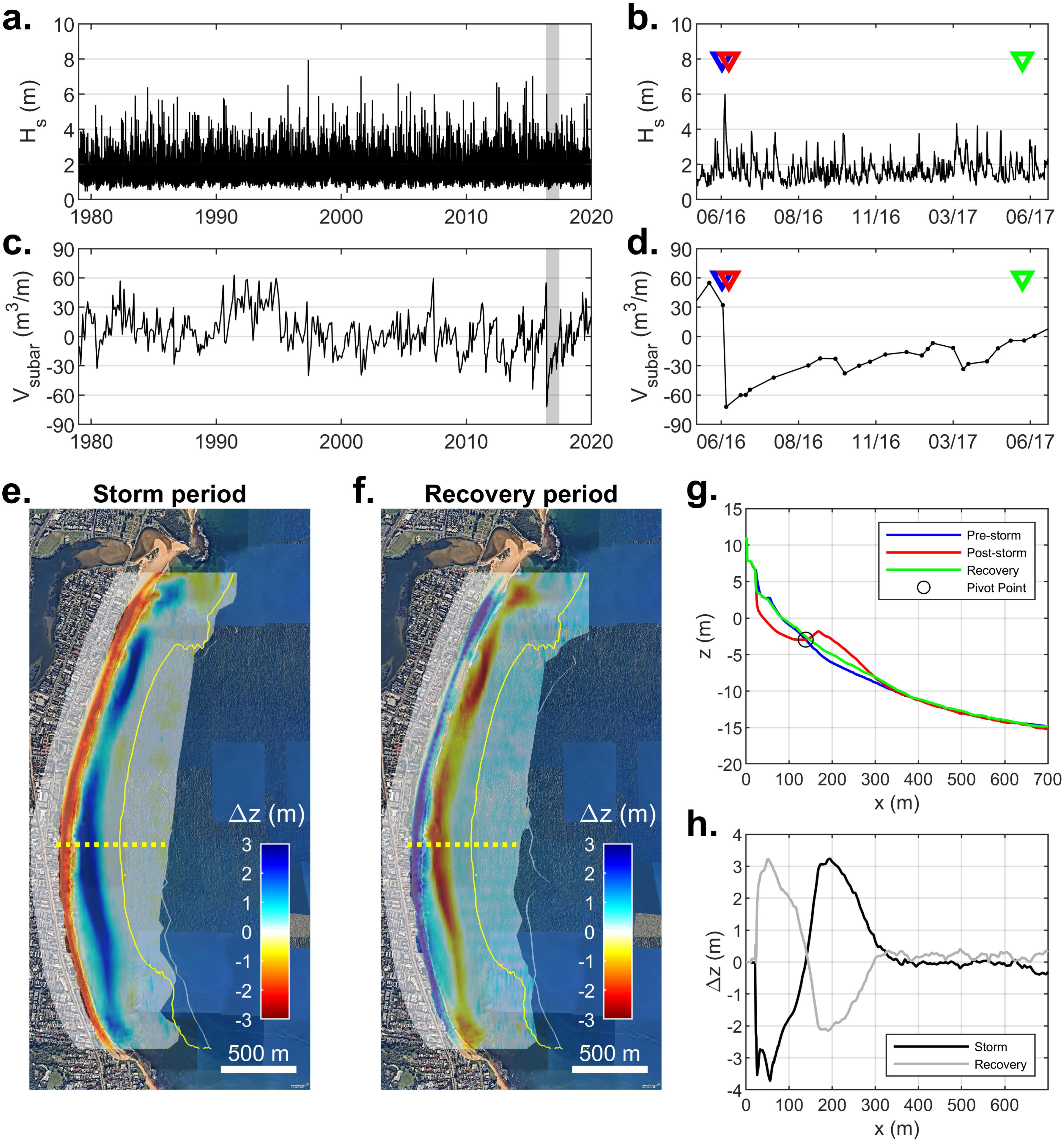

a.
b.
c.
d.
e.
f.
g.
h.
Storm period
Recovery period
Hs (m)
Vsubar (m3/m)
1980
1990
2000
2010
2020
06/16
08/16
11/16
03/17
06/17
Δz (m)
500 m
Pre-storm
Post-storm
Recovery
Pivot Point
z (m)
x (m)
Storm
Recovery

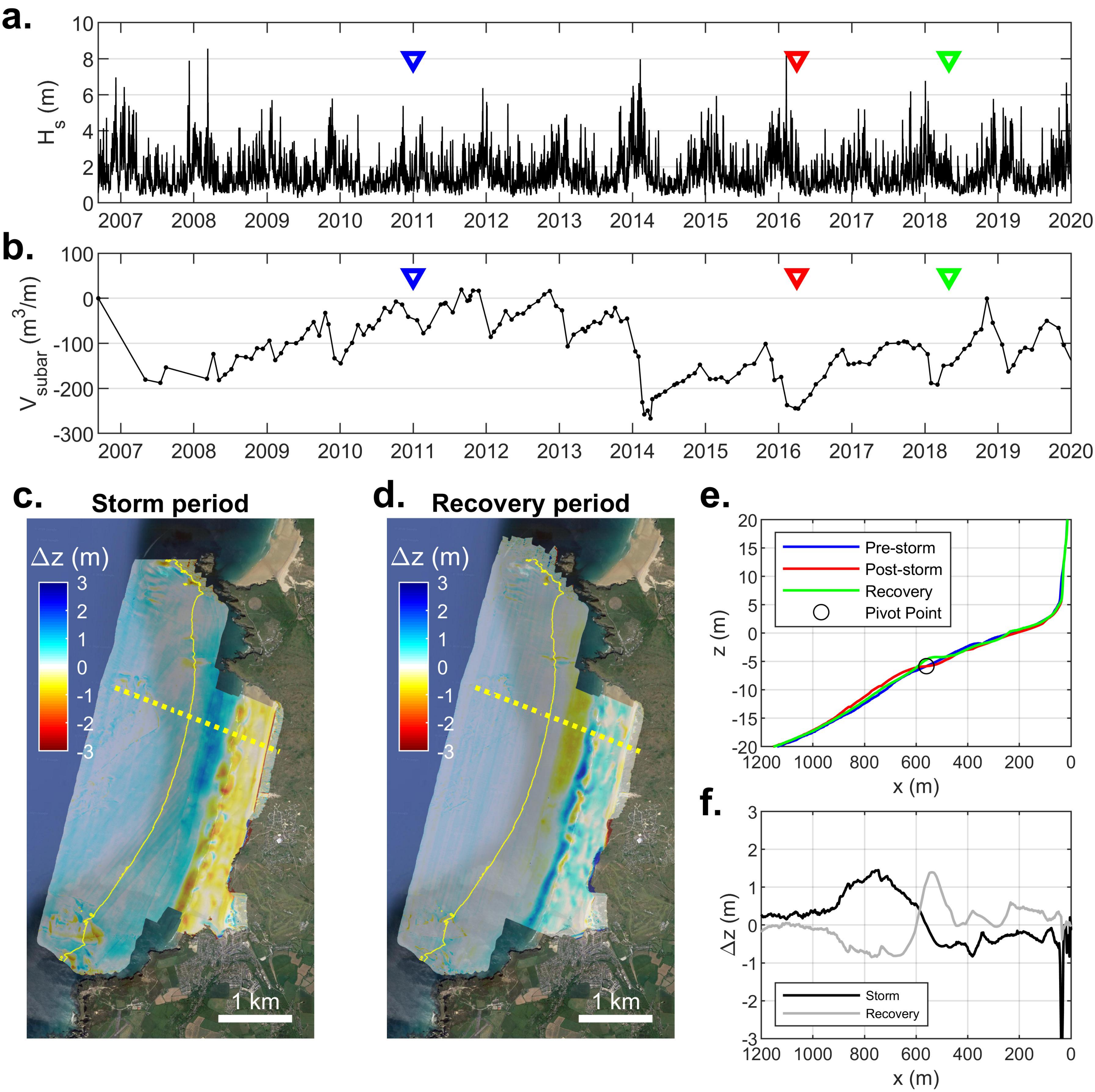

a.
H_s (m)
b.
V_{subar} (m^3/m)
2007 2008 2009 2010 2011 2012 2013 2014 2015 2016 2017 2018 2019 2020
c.
Storm period
Δz (m)
1 km
d.
Recovery period
Δz (m)
1 km
e.
Pre-storm
Post-storm
Recovery
Pivot Point
z (m)
x (m)
f.
Storm
Recovery
Δz (m)
x (m)

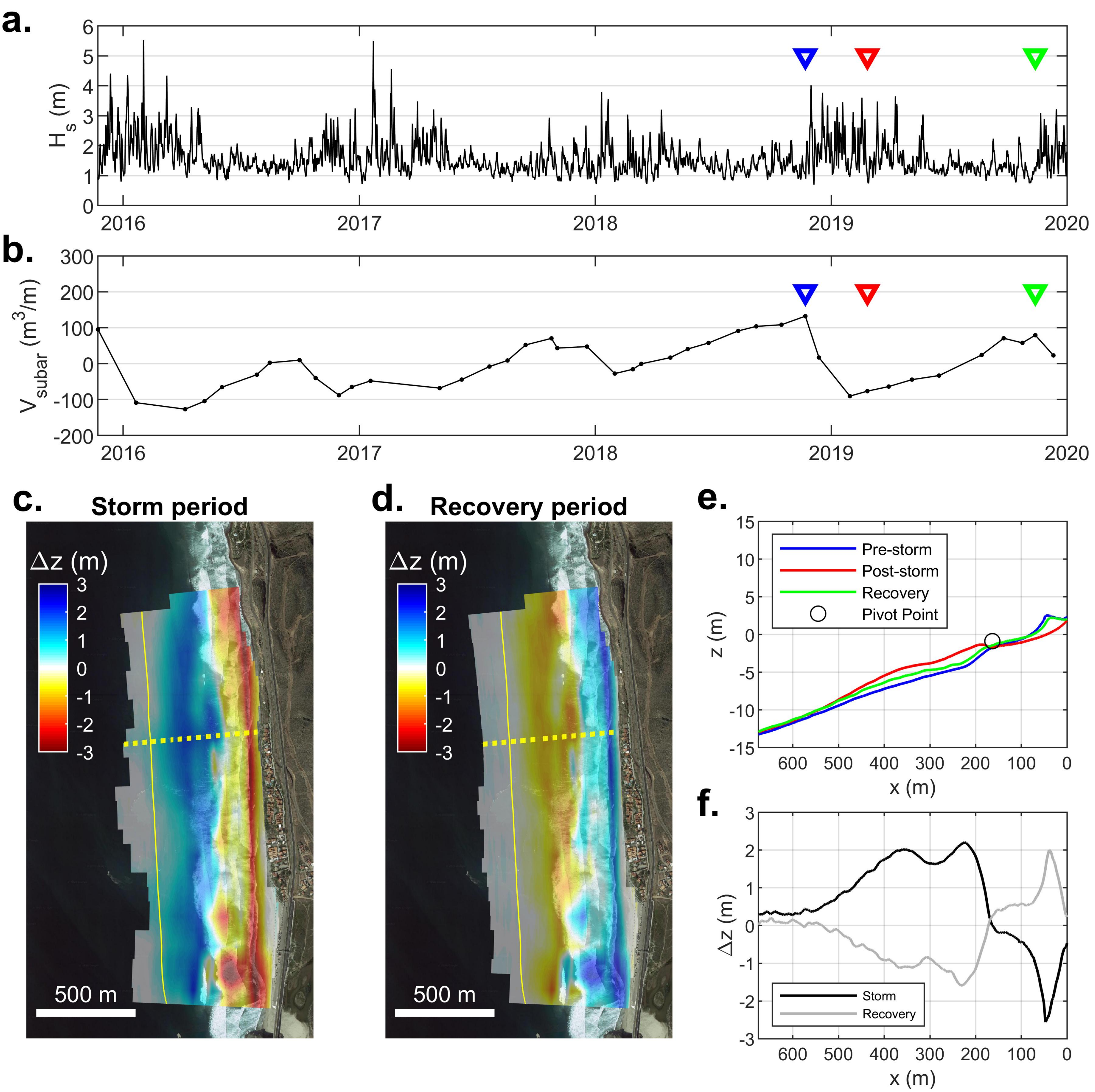

a.
H_s (m)
0
1
2
3
4
5
6
2016
2017
2018
2019
2020
b.
V_{subar} (m^3/m)
300
200
100
0
-100
-200
2016
2017
2018
2019
2020
c.
Storm period
Δz (m)
3
2
1
0
-1
-2
-3
500 m
d.
Recovery period
Δz (m)
3
2
1
0
-1
-2
-3
500 m
e.
z (m)
15
10
5
0
-5
-10
-15
Pre-storm
Post-storm
Recovery
Pivot Point
600
500
400
300
200
100
0
x (m)
f.
Δz (m)
3
2
1
0
-1
-2
-3
Storm
Recovery
600
500
400
300
200
100
0
x (m)

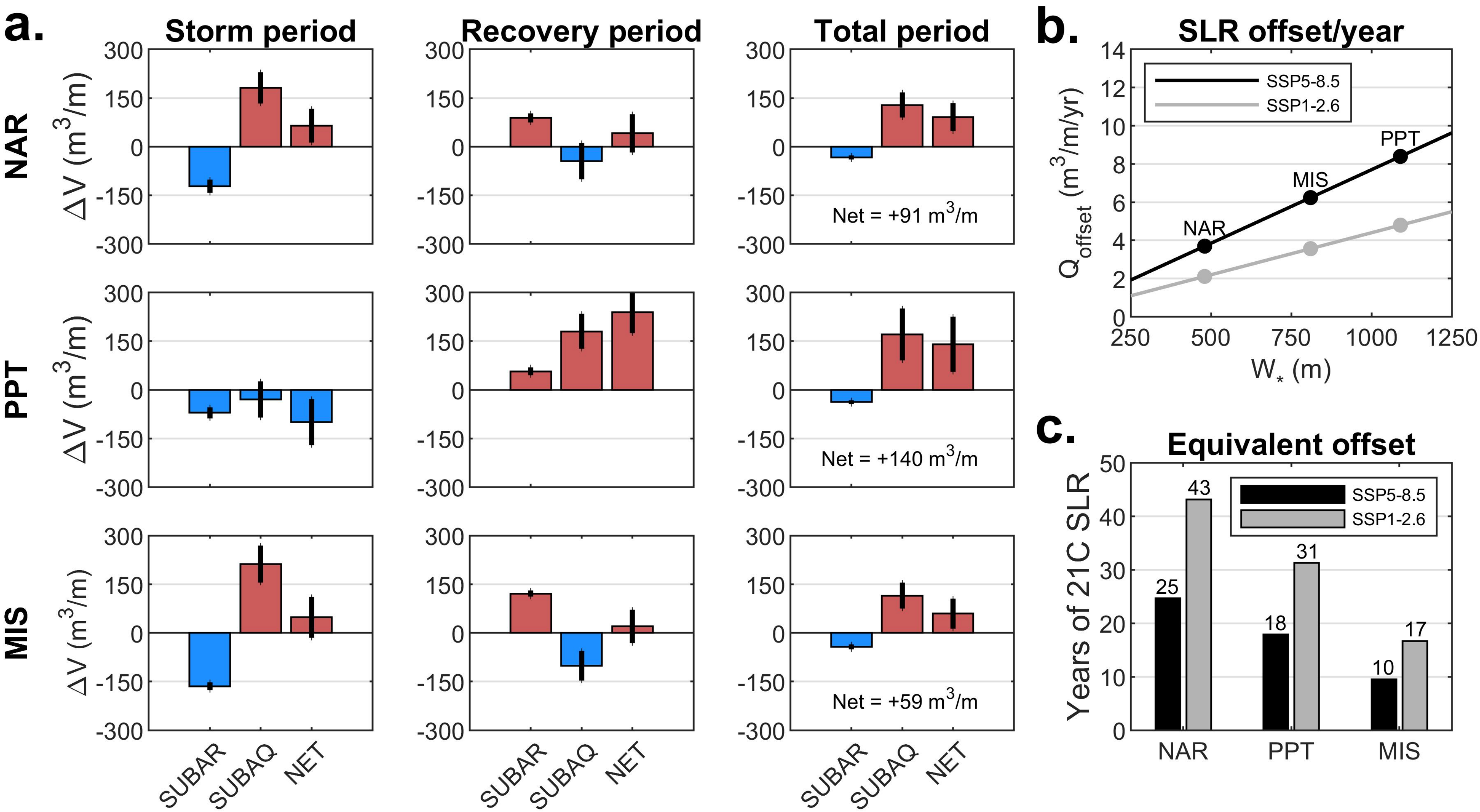

a.
Storm period
Recovery period
Total period
NAR
PPT
MIS
ΔV (m3/m)
Net = +91 m3/m
Net = +140 m3/m
Net = +59 m3/m
SUBAR
SUBAQ
NET
b.
SLR offset/year
SSP5-8.5
SSP1-2.6
Qoffset (m3/m/yr)
W* (m)
c.
Equivalent offset
Years of 21C SLR

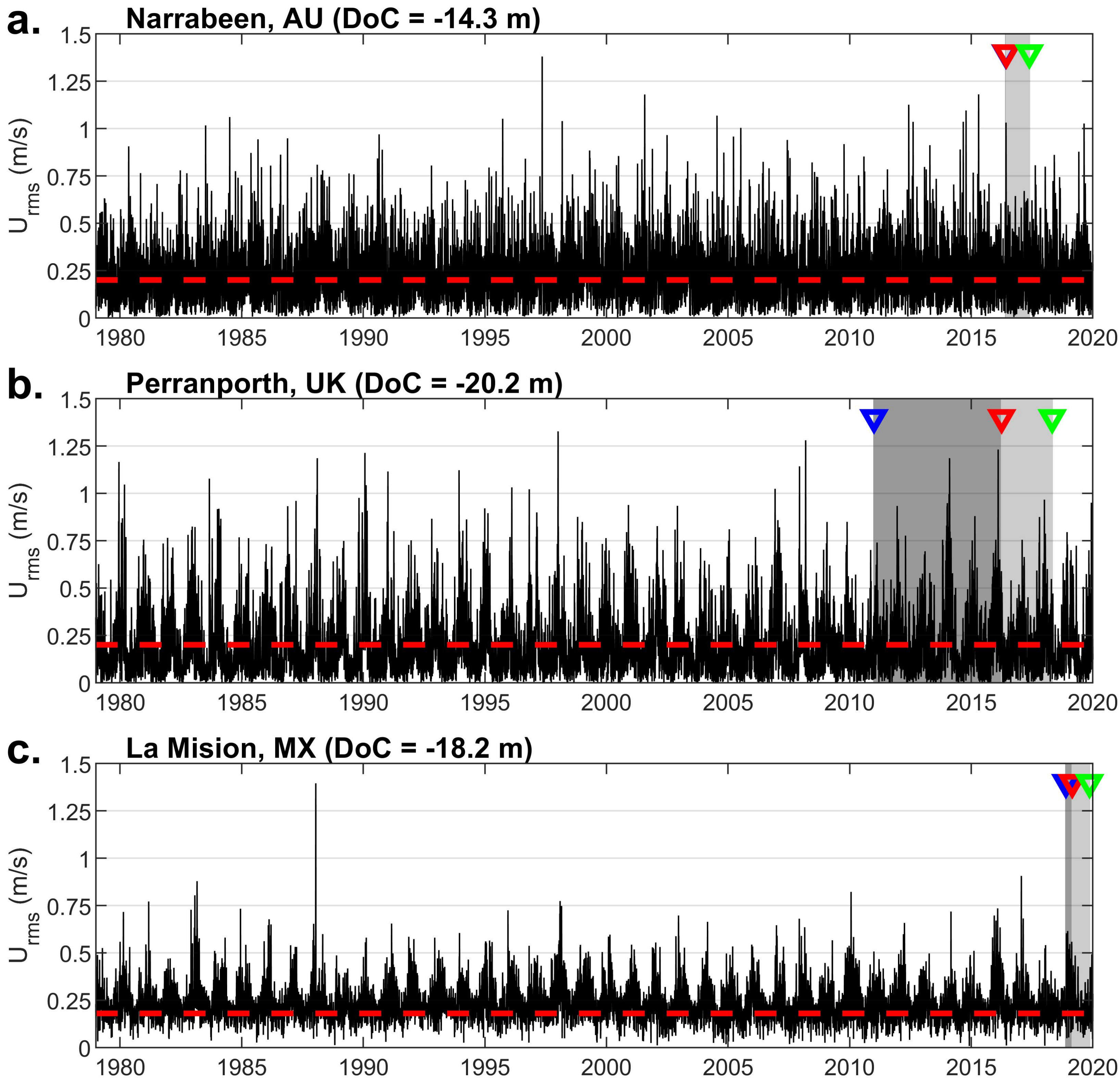
a.
Narrabeen, AU (DoC = -14.3 m)
b.
Perranporth, UK (DoC = -20.2 m)
c.
La Mision, MX (DoC = -18.2 m)
U_{rms} (m/s)
0
0.25
0.5
0.75
1
1.25
1.5
1980
1985
1990
1995
2000
2005
2010
2015
2020